The Astrophysical Journal, 809:150 (11pp), 2015 August 20 doi:10.1088/0004-637X/809/2/150

PROBING MAGNETIC FIELDS AT THE BASE OF THE SOLAR CONVECTION ZONE WITH MERIDIONAL FLOWS

Zhi-Chao Liang and Dean-Yi Chou
Physics Department, National Tsing Hua University, Hsinchu, 30013, Taiwan; chou@phys.nthu.edu.tw
Received 2015 April 16; accepted 2015 July 9; published 2015 August 19

ABSTRACT

Solar magnetic fields are responsible for most of the activities on the Sun. Many theories predict that it is generated by a dynamo near the base of the convection zone (BCZ), located at $0.71R_\odot$. In this study, we use the solar-cycle variations of the meridional flow to probe magnetic field variations near the BCZ. A helioseismic time-distance method is used to measure the travel-time difference between opposite directions in meridional planes, which reflects the meridional flow at different depths. Two systematic effects, the surface magnetic effect and the center-to-limb effect, are removed. Using *Solar and Heliospheric Observatory*/Michelson Doppler Imager data, we measure the latitudinal distribution of travel-time difference for different travel distances, corresponding to meridional flow signals in the solar interior down to $0.54R_\odot$, over 15 years, including two solar minima and one maximum. The travel-time differences at the maximum and the minimum behave differently in three different depth ranges. The travel-time difference at the maximum is greater than that at the minimum above the BCZ, while it is smaller around the BCZ; both are close to zero below the BCZ. The difference in the travel-time difference between the maximum and the minimum changes about 0.1 s from the region above the BCZ to the region around the BCZ, corresponding to a change in flow velocity of about $10\,\mathrm{m\,s^{-1}}$ around the BCZ. We tend to attribute this change in the meridional flow to the variation in the magnetic field from the minimum to the maximum near the BCZ.

Key words: Sun: activity – Sun: evolution – Sun: helioseismology – Sun: interior – Sun: magnetic fields – Sun: oscillations

1. INTRODUCTION

The solar magnetic field is responsible for most of the activities on the Sun. How and where the solar magnetic field is generated is a longstanding and unanswered question. Most theoretical studies predict that the solar magnetic field is generated by a dynamo near the base of the convection zone (BCZ) and rises to the surface as active regions (Ossendrijver 2003; Usoskin & Mursula 2003; Miesch 2005; Fan 2009; Charbonneau 2010; Choudhuri 2011). Many attempts have been made to detect the magnetic field at the BCZ, but no consistent and confirmed evidence has been found (Baldner & Basu 2008 and references therein). For example, Dziembowski & Goode (1989) have inferred a toroidal field of $(2 \pm 1) \times 10^6$ Gauss near the BCZ from measured frequency splitting. Other studies using inversion of mode frequencies have not found signals related to the magnetic field at the BCZ and placed an upper limit on some physical quantities near the BCZ, such as the field strength $B < 3 \times 10^5$ Gauss (Antia et al. 2000) and $\delta c/c < 3 \times 10^{-5}$ (Eff-Darwich et al. 2002), where δc is the change in sound speed at the BCZ between maximum and minimum. Chou & Serebryanskiy (2005) and Serebryanskiy & Chou (2005), using a smoothing method on mode frequency to remove the surface effect, have reported $\delta c^2/c^2 \approx (2\text{–}6) \times 10^{-5}$ between the maximum and minimum. Baldner & Basu (2008), using principal component analysis, obtained $\delta c^2/c^2 = (7.23 \pm 2.08) \times 10^{-5}$ at the BCZ, related to solar-cycle variations. Instead of using p-mode frequencies as in the above studies, Chou & Serebryanskiy (2002) have reported a value of $(9 \pm 4) \times 10^{-6}$ for the relative change in mean travel time between the maximum and minimum for the wave path with the lower-turning layer at the BCZ.

In this study, we use the measured solar-cycle variations of the meridional flow to probe the magnetic field near the BCZ. The meridional flow is a large-scale axisymmetric circulating flow in meridional planes. It moves poleward on the surface and penetrates into the interior. It was originally proposed to balance the latitudinal dependence of energy transport due to rotation (Durney & Roxburgh 1971).

Surface measurements have shown that the speed of poleward motion on the surface versus latitude has an approximate sine-shape distribution, with a peak magnitude of $10\text{–}20\,\mathrm{m\,s^{-1}}$ (Duvall 1979; Howard & Gilman 1986; Hathaway & Rightmire 2010; Ulrich 2010). The subsurface meridional flow, measured with helioseismic methods, extends through the entire solar convection zone (Giles et al. 1997; Giles 1999). The meridional flow plays an important role in the dynamics of the Sun (Wang et al. 1989). It can also be used to probe the temporal variations of the solar interior (Chou & Dai 2001; Beck et al. 2002; Chou & Ladenkov 2005). At solar maximum, the meridional flow has a smaller magnitude on the surface (Komm et al. 1993; Meunier 1999; Hathaway & Rightmire 2010) and in the upper convection zone (Chou & Dai 2001).

Here we use the time-distance method in helioseismology to measure meridional flow signals at different depths down to $0.54R_\odot$. A resonant solar acoustic mode (p-mode wave) is trapped and multiply reflected in a cavity between the surface and a layer in the solar interior. The acoustic signal emanating from a point on the surface propagates downward to the bottom of the cavity and back to the surface at a distance from the original point. Different p-modes have different paths and arrive at the surface with different travel times and distances. The relation between the travel time and distance can be measured with the time-distance technique using the temporal

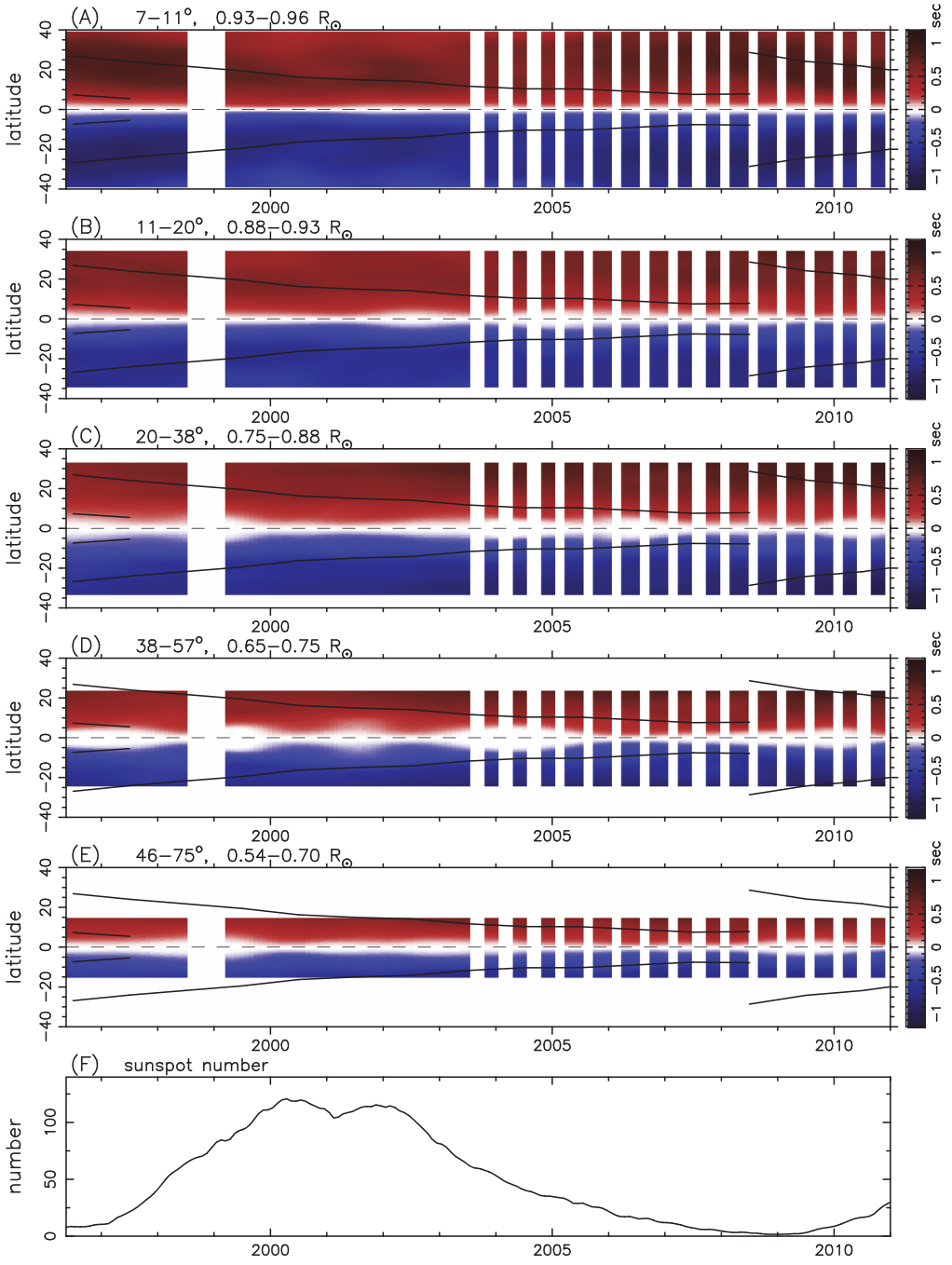

Figure 1. Panels (A)–(E): travel-time difference $\delta\tau$, with magnetic fields greater than 50 G removed, as a function of latitude and time for different travel distances. The range of travel distances and the corresponding radii of lower-turning layers from ray approximation are indicated at the top of each panel. The positive value (red) corresponds to northward motion and the negative value (blue) corresponds to southward motion. Only the antisymmetric component is kept (see the text). The unit in the color bar is second. A Gaussian smoothing, with FWHM $= 7\overset{\circ}{.}2$ in latitude and one year in time, is applied to show the large-scale variations. The black line marks the center of the active latitudes. The tick of year indicates the beginning of the year. The blank in 1998 and 1999 is caused by the spacecraft loss. Half of the data after 2003 July, when the MDI instruments flipped 180°, are not used here to ensure consistency. Panel (F): sunspot numbers vs. time. This figure is cited from Liang & Chou (2015).

cross-correlation between two points on the surface (Duvall et al. 1993). The wave associated with a greater travel distance penetrates deeper into the interior. Thus the waves of different travel distances can be used to probe different depths of the solar interior.

The travel time depends on the wave speed and the flow speed along the wave path. The mean of the travel times of opposite directions only depends on the wave speed along the wave path, and the difference, denoted as $\delta\tau$, depends only on the flow speed (Duvall et al. 1996; Kosovichev 1996). Here we measure $\delta\tau$ for a pair of points at the same longitude to study meridional flows (Giles et al. 1997). Using different pairs at different latitudes for different travel distances at different times allows us to study the solar-cycle variations of meridional flow as a function of latitude and depth.

The data and our analysis are described in Section 2. In Section 3, the removal of two systematic effects, the surface magnetic effect and the center-to-limb effect, is discussed. In

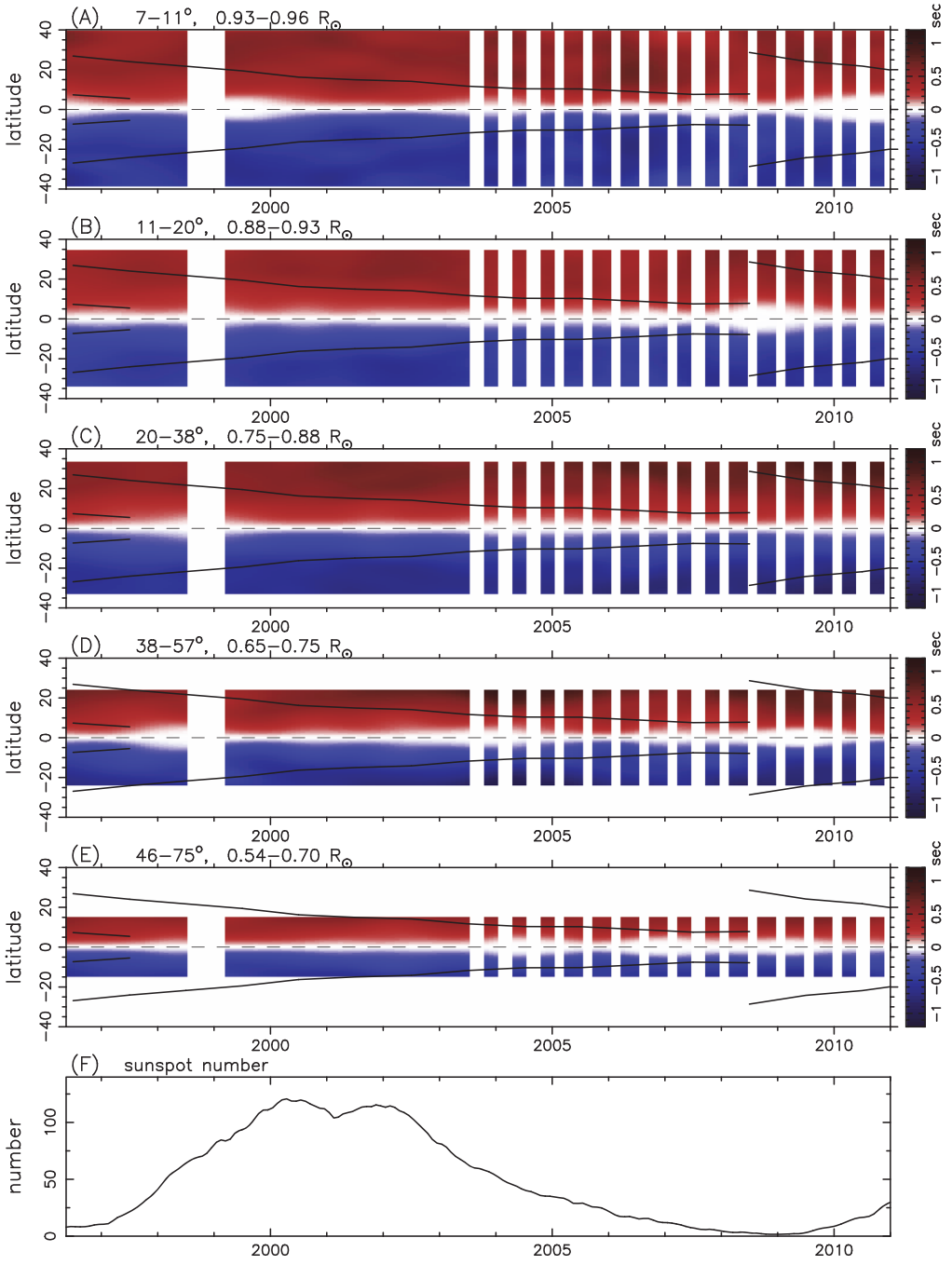

Figure 2. Same as Figure 1, but the $\delta\tau$ is measured in the east–west direction.

Section 4, the solar-cycle variations of travel-time difference $\delta\tau$ as a a function of latitude and depth are discussed.

2. DATA AND ANALYSIS

We use 15 years of (1996–2010) data taken with the Michelson Doppler Imager (MDI) on board the *Solar and Heliospheric Observatory* spacecraft (Scherrer et al. 1995). They are full-disk Doppler images of 192×192 pixels, sampled at a rate of one image per minute. Each time series of 24 hr is analyzed separately. The travel-time difference analysis procedure is the same as Liang & Chou (2015), and is described as follows. (1) A temporal filter is applied to remove signals below 1.5 mHz; a Hann-window is applied to smooth the transition region, 1.5–2 mHz. No other filter is applied in this study to avoid the spreading of the influence of magnetic regions because magnetic regions will be removed in following analyses. (2) Each image is transformed into the heliographic longitude-latitude coordinates with a step size of $0\overset{\circ}{.}6$ in both directions. (3) The surface differential rotation is removed (Chou et al. 2009). (4) The cross-correlation function (CCF) is computed on an arc-to-arc basis. For each point, two arcs of 30° in the north–south direction, with the same distance to the central point, are selected. The CCF between a pair of opposite points on the two arcs is computed, and then the CCFs of the different pairs on the arcs are averaged. The result is assigned to the central point. (5) The computation of the arc-averaged

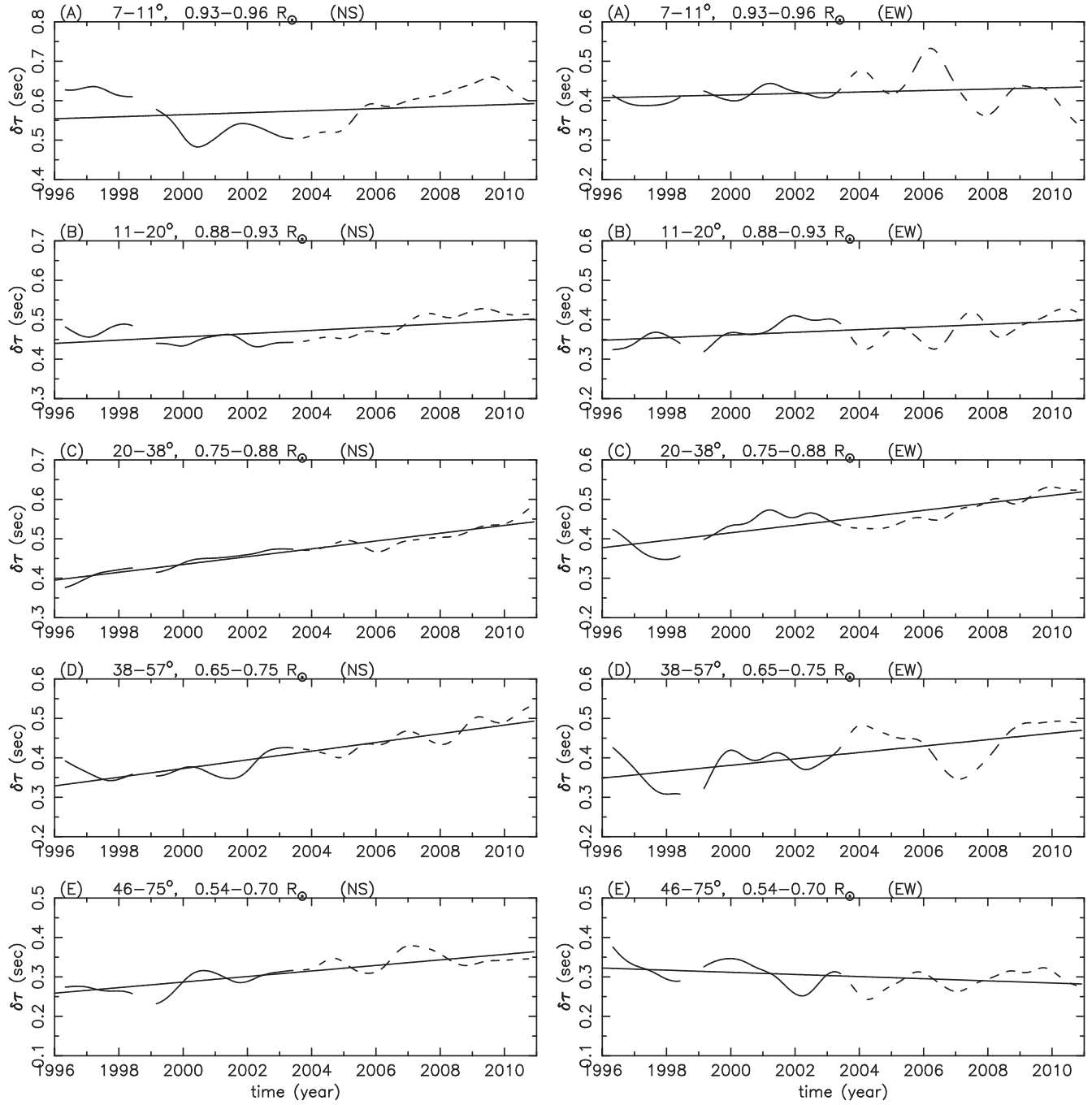

Figure 3. Left panels: north–south $\delta\tau$ averaged over latitude for five different depths. The latitudinal average for each depth is over the available range of latitudes shown in Figure 1. The straight line is the linear fit. Right panel: east–west $\delta\tau$ averaged over latitude.

CCF is repeated for different central points. Each step is $0\overset{\circ}{.}6$ in longitude and latitude. For each latitude, the CCF's are averaged over $\pm 45^\circ$ longitude to enhance the signal-to-noise ratio. (6) The above procedure of computing the CCF is repeated for each 24 hr time series, then the CCF is averaged over one month to enhance the signal-to-noise ratio before determining the travel time. (7) The northward and southward travel times are determined from the monthly averaged CCF. Two different methods are used here to determine the travel time. One is fitting the instantaneous phase of the CCF (Chou & Serebryanskiy 2002). The other method is measuring the relative shift between each CCF and the CCF averaged over the quiet Sun (Gizon & Birch 2002). The difference between the two results is negligibly small in this study. In the following discussion, we present only the result using the former method. (8) The difference between opposite-direction travel times $\delta\tau$ carries information regarding meridional flows along the wave path. The convention is that the positive $\delta\tau$ corresponds to the northward motion and the negative corresponds to the southward motion. (9) The above procedure is repeated for different latitudes, travel distances, and times to obtain $\delta\tau$ as a function of latitude, travel distance, and time. To ensure consistency, half of the data after 2003 July, when the MDI instruments flipped 180°, are not used in this study.

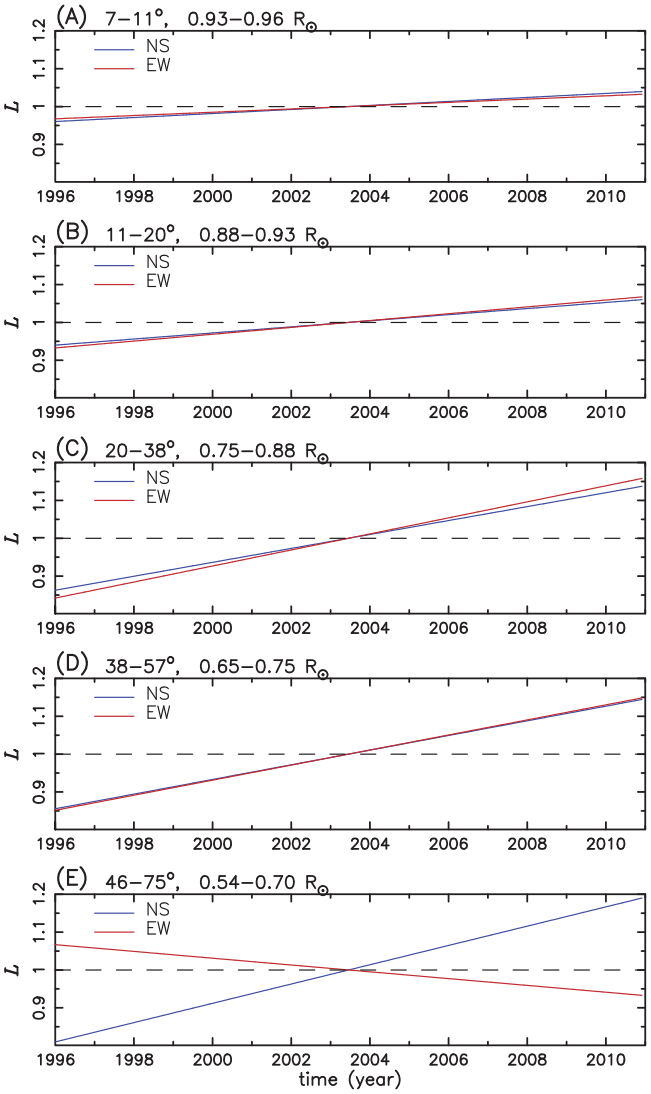

Figure 4. $L(t)$, normalized linear fit in Figure 3, vs. time for both the north–south $\delta\tau$ (blue) and the east–west $\delta\tau$ (red). The value at the middle time (2003.06) is set to unity.

The travel-time difference $\delta\tau$ is proportional to a weighted average of the flow velocity along the wave path, but the main contributions come from the lower-turning layer, unless there is a vertical flow near the surface where the wave path is almost vertical (Giles 1999). Note that the meridional flow near the surface is predominantly horizontal. Therefore, $\delta\tau$ mainly reflects the meridional flows around the lower-turning layer for each travel distance. The larger the travel distance, the deeper the lower-turning layer.

3. REMOVAL OF SYSTEMATIC EFFECTS

To accurately measure the travel-time difference $\delta\tau$, one needs to remove systematic effects. So far, two systematic effects on the measured $\delta\tau$ are known, and will be discussed in this section. One is the surface magnetic effect and the other is the center-to-limb effect.

3.1. Surface Magnetic Effect

The study of Liang & Chou (2015) has shown that the surface magnetic field creates a signal in additional to the large-scale meridional flow in the measured $\delta\tau$. This additional signal could be explained by effective downflows inside magnetic regions. These effective downflows could be the real downflows inside the magnetic regions (Duvall et al. 1996; Kosovichev 1996), or the signal generated by the complication of the Doppler signal measured in the magnetic regions and appearing in the measured $\delta\tau$, or a combination of both. These local effective downflows are unrelated to the large-scale meridional flow. In this study, we remove the surface magnetic effect by excluding the magnetic regions with a field strength greater than a threshold. Liang & Chou (2015) have shown that a threshold of 50 G could remove most of the surface magnetic effect, because the difference between the results with a threshold of 35 G and 50 G is negligibly small. Thus, here we use a threshold of 50 G to remove the surface magnetic effect.

The travel-time difference $\delta\tau$ is averaged over a travel distance range to enhance the signal-to-noise ratio. The results of five travel distance ranges, as a function of latitude and time, are shown in Figure 1. The range of the travel distance from averaging and the corresponding range of the lower-turning layer are shown at the top of each panel. It should be noted that the lower-turning layer is computed based on the ray approximation. The actual depth range sampled by the wave packet associated with each travel distance is rather broad. Only the antisymmetric component of $\delta\tau$ with respect to the equator is kept to remove contamination from rotation caused by errors in the telescope pointing (Giles 1999; Beck et al. 2002). A Gaussian smoothing has been applied in the domains of time and latitude. The FWHMs in the temporal and latitudinal smoothings are one year and $7\overset{\circ}{.}2$, respectively.

Figure 1 shows that the $\delta\tau$ has some solar-cycle variations. However, it is rather different from the previous results in which the surface magnetic regions have not been removed in the analysis (Chou & Dai 2001; Beck et al. 2002; Chou & Ladenkov 2005; Kholikov & Hill 2014). The difference between the results with and without surface magnetic effects removed has been discussed in detail in Liang & Chou (2015). The solar-cycle variations of $\delta\tau$ in Figure 1 will be discussed in Section 4.

3.2. Center-to-limb Effect

The other systematic effect in the measured $\delta\tau$ has been first shown by Duvall & Hanasoge (2009). They have found that the measured $\delta\tau$ along the east–west direction, which is not affected by meridional flow, is nonzero. It is called the center-to-limb effect, though this name might not well reflect the phenomenon. This nonzero signal is also included in the measured $\delta\tau$ in the north–south direction. Zhao et al. (2012) have shown that the north–south $\delta\tau$s measured from different observables are rather different. After subtracting the east–west $\delta\tau$, the north–south $\delta\tau$s of different observables become closer. Thus, they have proposed that the center-to-limb effect could be empirically removed by subtracting the east–west $\delta\tau$, although the cause of the center-to-limb effect is unclear (Baldner & Schou 2012). It should be mentioned that the tests of Zhao et al. (2012) are carried out for the travel distances less than $3\overset{\circ}{.}84$, corresponding to the upper convection zone. In this study, we also adopt this empirical method to remove the center-to-limb effect.

The procedure to measure the $\delta\tau$ in the north–south direction described in Section 2 is repeated for the $\delta\tau$ in the east–west direction. Since the longitude and latitude are not geometrically

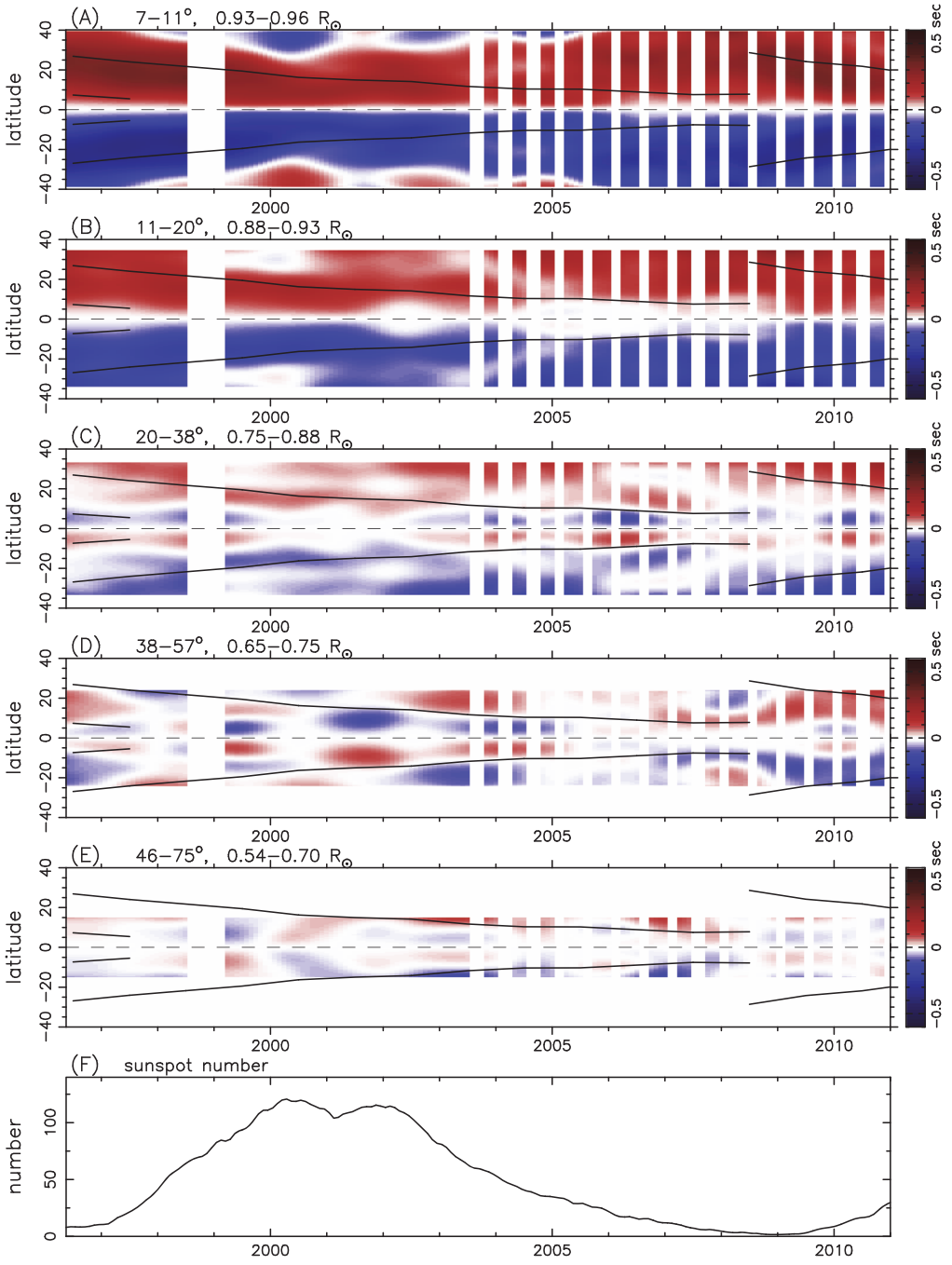

Figure 5. Results of subtracting the east–west $\delta\tau$ (Figure 2) from the north–south $\delta\tau$ (Figure 1). The color scale is different from that in Figures 1 and 2.

identical, to make their geometries identical, the directions in mapping into "longitude-latitude" coordinates are swapped such that the "longitude" is in the north–south direction and the "latitude" is in the east–west direction in our computer codes. Similar to the measurement of north–south $\delta\tau$, the magnetic regions above 50G are also excluded in the measurement of the east–west $\delta\tau$. The result of the east–west $\delta\tau$ is shown in Figure 2.

Unlike the north–south $\delta\tau$, the latitudinal dependence of east–west $\delta\tau$ does not change with the solar cycle as expected because the east–west $\delta\tau$ represents only the center-to-limb effect. However, the magnitude of the measured east–west $\delta\tau$ has a slow temporal variation. To demonstrate it, the latitude-averaged east–west $\delta\tau$s versus time at five different depths are shown in the right panels of Figure 3. There exists a long-term trend, which gradually increases with time, except for the deepest one (panel (E)). The magnitude of the north–south $\delta\tau$ also has a similar trend, which is shown in the left panels of Figure 3. The fluctuation of the east–west $\delta\tau$ is greater than that of the north–south $\delta\tau$ because the east–west $\delta\tau$ is averaged only over $\pm 15^\circ$ "longitude". The long-term variation is approximated by a linear function, shown by a solid line in each panel. Since the magnitudes of the north–south $\delta\tau$ and the east–west $\delta\tau$ are different, to compare the slow variations in the east–west and north–south directions, the linear function is normalized by the value at the middle time (2003.06). The

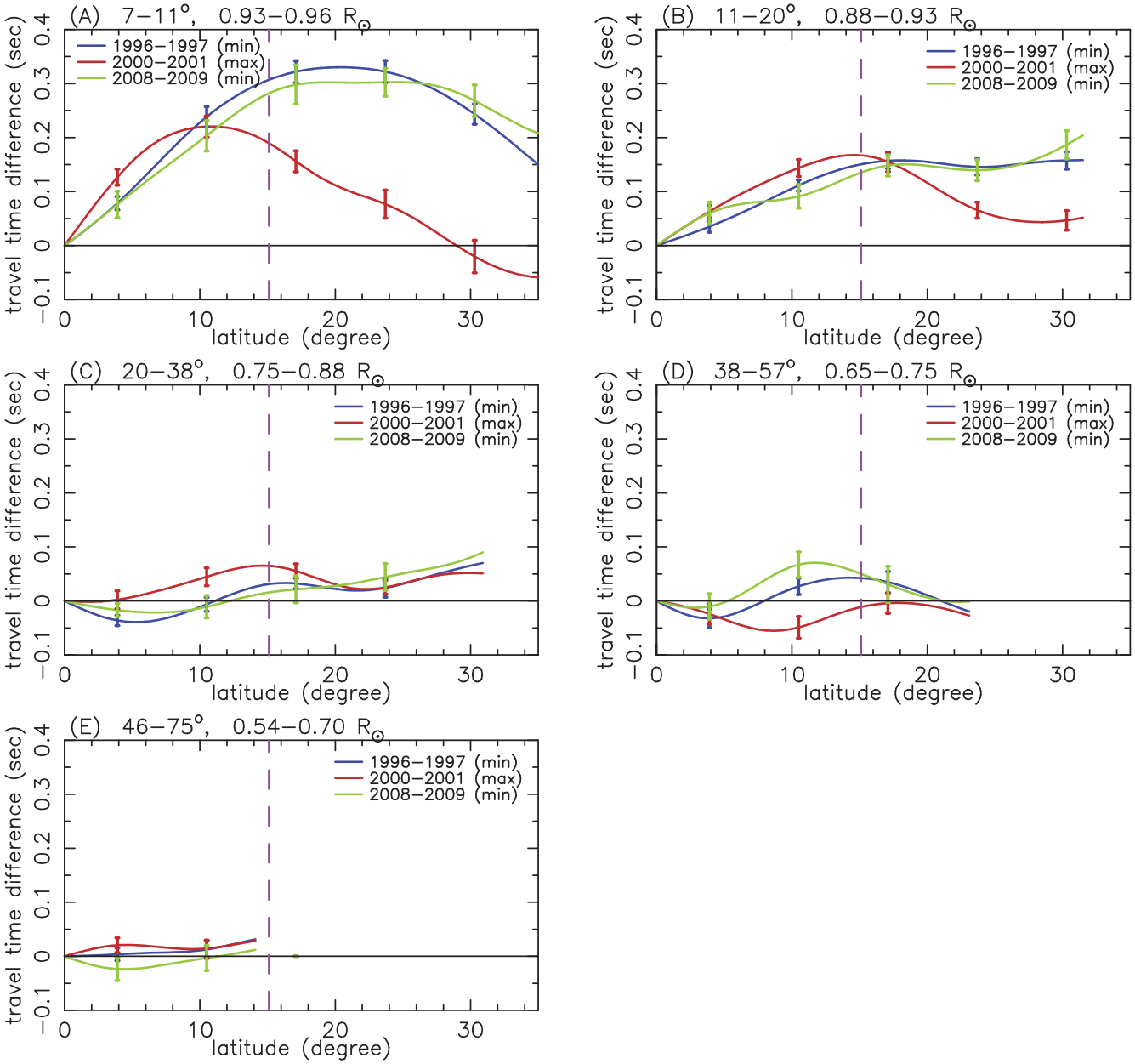

Figure 6. Averages of $\delta\tau$ in Figures 5(A)–(E) over three periods (two minima and one maximum) vs. latitude, respectively, at five depths. Only the northern hemisphere is shown here because we keep only the antisymmetric component. The vertical dashed line indicates the centroid of active latitudes at the maximum. The error is computed from the fluctuation in averaging (Giles 1999).

result, called $L(t)$, is shown in Figure 4. It is clear that the long-term trends of east–west $\delta\tau$ and north–south $\delta\tau$ are rather similar at all depths, except for the deepest one (panel (E)), which might be caused by the larger error in the east–west $\delta\tau$. We speculate that this slow linear increase in time in both the north–south $\delta\tau$ and the east–west $\delta\tau$ could be instrumental or due to calibration.

In this study, we use the function $\langle\delta\tau(\theta)\rangle L(t)$ to represent the center-to-limb variation, where $\langle\delta\tau(\theta)\rangle$ is the averaged latitudinal (θ) dependence of the east–west $\delta\tau$ over 15 years and $L(t)$ is the normalized linear function of time t for the east–west $\delta\tau$ shown in Figure 4. The center-to-limb effect is removed by subtracting $\langle\delta\tau(\theta)\rangle L(t)$ from the north–south $\delta\tau$ in Figure 1. For the deepest depth (panel (E)), $L(t)$ from the north–south $\delta\tau$ instead of the east–west $\delta\tau$ is used. The results after removing the center-to-limb effect are shown in Figure 5.

4. SOLAR-CYCLE VARIATIONS OF $\delta\tau$

The travel-time difference $\delta\tau$ in Figure 5 has different solar-cycle variations at different latitudes and depths. For a better comparison between the maximum and the minima, the $\delta\tau$s in Figures 5(A)–(E) are averaged over the maximum and the two minima, and their latitudinal dependencies are shown in Figures 6(A)–(E), respectively. Only the northern hemisphere is shown because we keep only the antisymmetric component. In Figure 6, the $\delta\tau$s at two minima are similar at all depths, but they are different from that at the maximum.

Figure 6(A) shows that the $\delta\tau$'s at the maximum and the minima have different magnitudes and shapes. The overall

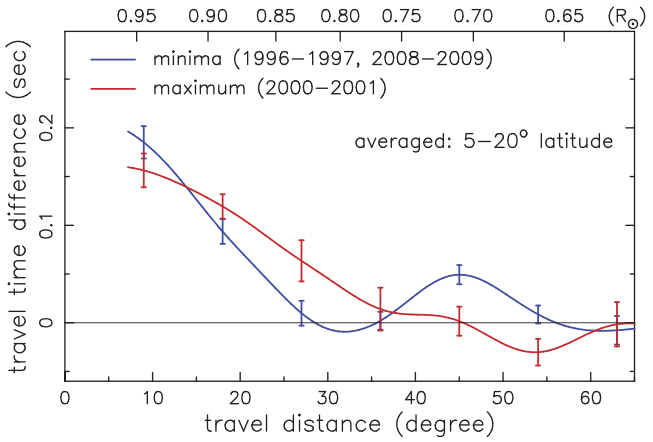

Figure 7. Average of $\delta\tau$ over a 5°–20° latitude and over two minima and the maximum vs. travel distance (depth). A Gaussian smoothing, with FWHM = 9° in travel distance, is applied here. The numeric label at the top of the panel is the radius of the lower-turning layer in units of solar radius.

magnitude of $\delta\tau$ at the maximum is smaller than that of the minima. This phenomenon is consistent with the previous studies with surface measurements (Hathaway & Rightmire 2010) and the $\delta\tau$ measurements for the travel distance 2°–6° (Chou & Dai 2001). Another phenomenon shown in Figure 6(A) is that the $\delta\tau$ at the maximum is enhanced relative to the minima in the regions below the active latitudes and reduced in the regions above the active latitudes. Because of the smaller overall magnitude at the maximum, the enhancement below the active latitudes is smaller than the reduction above the active latitudes.

Figure 5(A) also clearly shows the reduction in $\delta\tau$ at the maximum above the active latitudes; the enhancement below the active latitudes is less apparent because of the small difference and the color scale. The reduction in $\delta\tau$ above the active latitudes correlates with surface activities. It is clearly present from 1998 to 2005 and also visible in 2010, the beginning of cycle 24. The reduction in $\delta\tau$ above the active latitudes and the enhancement below them suggests the presence of flows moving toward the active latitudes, superposed on the background meridional flows. This phenomenon is consistent with previous studies with surface measurements (Hathaway & Rightmire 2011) and the results from helioseismic inversion for the regions shallower than 0.98 $R_\odot$ (Haber et al. 2002; Basu & Antia 2003; Zhao & Kosvichev 2004). The same phenomenon also appears in Figures 5(B) and 6(B), although weaker.

The enhancement in $\delta\tau$ at the maximum relative to the minima below the active latitudes is still present in Figure 6(C), but the reduction above the active latitudes disappears. The most striking phenomenon is that the $\delta\tau$ in Figure 6(D), corresponding to the depth around the BCZ, has a behavior opposite to above three layers (Figures 6(A)–(C)): the $\delta\tau$ at the maximum is negative and smaller than those at the two minima below the active latitudes. In Figure 6(E), below the BCZ, the $\delta\tau$s in all three periods are close to zero.

For a better comparison of the depth dependence of $\delta\tau$ between the maximum and the minima, $\delta\tau$ is averaged over a 5°–20° latitude, where the difference between the maximum and the minima is most significant, and over the maximum and the minima for each travel distance. The averaged $\delta\tau$s at the maximum and the minima versus travel distance (depth) are shown in Figure 7. A Gaussian smoothing, with FWHM = 9° in travel distance, is applied here. The radius of lower-turning layer associated with each travel distance computed from the ray approximation is labeled at the top of the panel. In the upper convection zone ($R_\odot > 0.92$), the $\delta\tau$ at the maximum is smaller than that at the minima. It is caused by the smaller overall magnitude at the maximum relative to the minima in the upper convection zone. Below this upper convection zone, the difference in $\delta\tau$ between the maximum and the minima behaves differently in three different regions: above the BCZ, around the BCZ, and below the BCZ. The $\delta\tau$ at the maximum is greater than that at the minima in the region above the BCZ (0.75–0.92 $R_\odot$), while it is smaller around the BCZ (0.65–0.75 $R_\odot$). Below the BCZ (<0.65 $R_\odot$), both are close to zero. The difference in $\delta\tau$ between the maximum and the minimum changes about 0.1 s from the region above the BCZ to the region around the BCZ. Figure 7 is consistent with Figures 6(A)–(E).

The above characteristics of the solar-cycle variations of $\delta\tau$ shown in Figures 6 and 7 should not be affected by the center-to-limb effect because it only reduces the magnitude and slightly modifies the latitudinal dependence. The phenomenon that the difference in $\delta\tau$ between the maximum and the minima changes the sign around the BCZ also exists before removing the center-to-limb effect. To demonstrate it, we plot, as in Figure 6, the latitudinal dependence at the maximum and the two minima for the $\delta\tau$ without the center-to-limb correction in Figure 8. (The slow linear increase in $\delta\tau$, $L(t)$, has been removed in Figure 8.) Although the magnitudes of $\delta\tau$ in Figures 6 and 8 are different, the behavior of the characteristic difference between the maximum and the minima in Figure 8 is similar to that in Figure 6.

As Figure 7, we also plot the depth dependence of averaged $\delta\tau$ over a 5°–20° latitude at the maximum and the minima for the $\delta\tau$ without the center-to-limb correction in Figure 9. Besides the magnitude of $\delta\tau$ being different from that in Figure 7, the behavior of the difference between the maximum and the minima in Figure 9 is similar to that in Figure 7: $\delta\tau$ at the maximum is greater than that at the minima in the layers above 0.75 $R_\odot$, while it is smaller in 0.65–0.75 $R_\odot$, around the BCZ; below 0.65 $R_\odot$, both values are close.

5. SUMMARY AND DISCUSSION

The interesting phenomenon in this study can be summarized in Figures 6 and 7, which show that the difference in the $\delta\tau$ between the maximum and the minima changes from a positive value above the BCZ to a negative value around the BCZ, and becomes zero below the BCZ. In this study, we have removed two known systematic effects on $\delta\tau$: the surface magnetic effect and the center-to-limb effect. Although we cannot rule out the existence of other unknown systematic effects, they would not affect the conclusion that there exists a change in the difference between the maximum and the minima around the BCZ shown in Figures 6 and 7, as long as the unknown systematic effects are not time dependent.

Since the $\delta\tau$ discussed here is computed by removing the magnetic regions above 50G, a question can be raised: is it possible that the change in the difference between the maximum and the minima around the BCZ is caused by the residual of the surface magnetic effect, namely, by the magnetic regions below 50G? To see how the surface magnetic effect affects the behavior of $\delta\tau$ around the BCZ, we compare

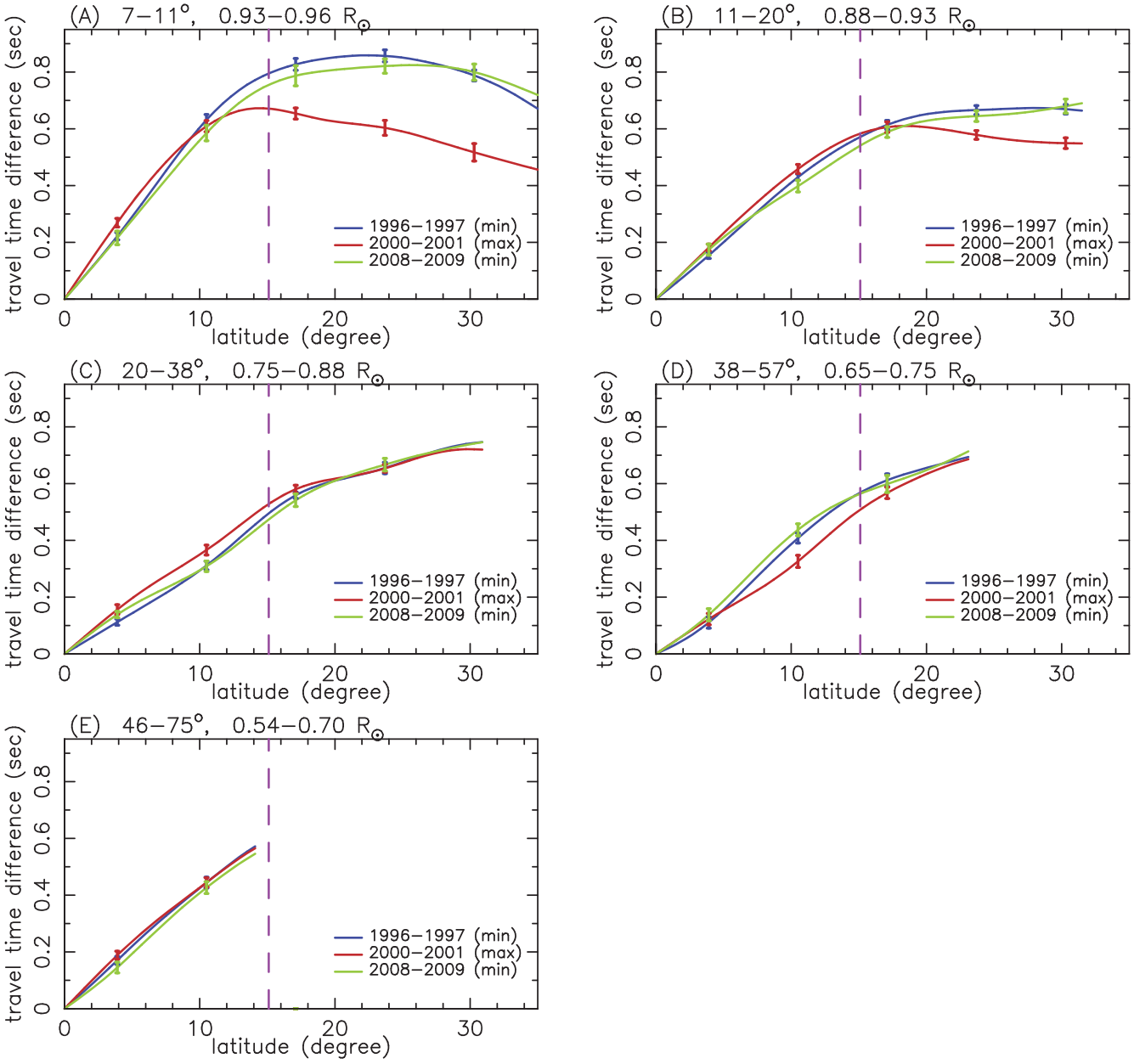

Figure 8. Same as Figure 6, but for the $\delta\tau$ without the center-to-limb correction.

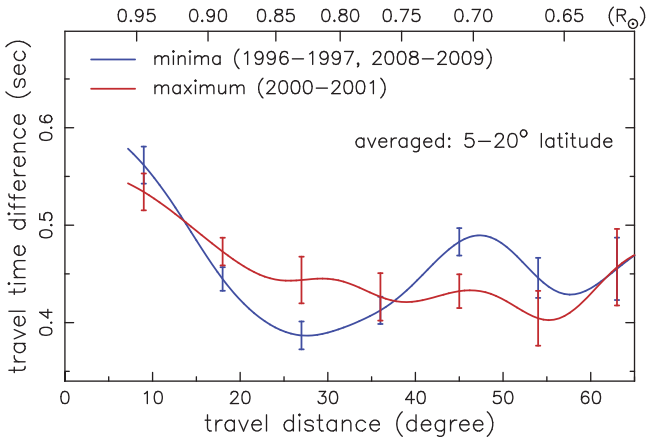

Figure 9. Same as Figure 7, but for the $\delta\tau$ without the center-to-limb correction.

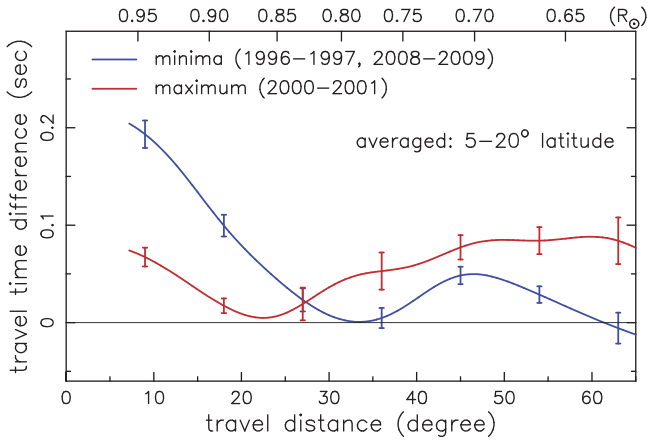

Figure 10. Same as Figure 7, but for the $\delta\tau$ without surface magnetic regions removed.

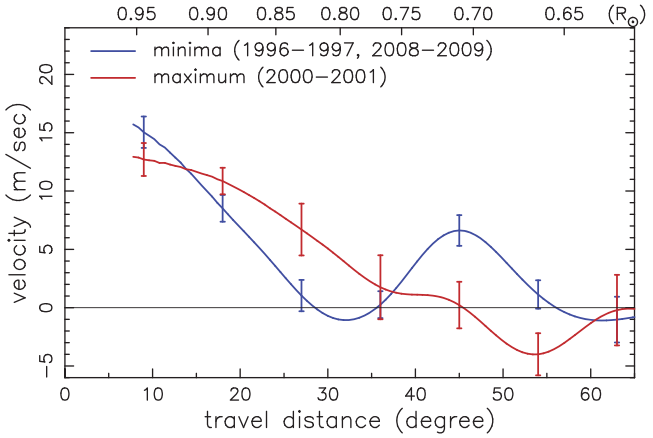

Figure 11. Horizontal component of meridional flow velocity vs. travel distance (depth) from an order-of-magnitude estimate based on Equation (1) and the $\delta\tau$ in Figure 7. It is assumed that only the flow in a region near the lower-turning point has a contribution to $\delta\tau$. The error bar is computed from the error bar of $\delta\tau$ in Figure 7. The numeric label at the top of the panel is the radius of lower-turning layer in units of solar radius. It should be warned that this estimate could be rather different from inversion results.

the $\delta\tau$s at the maximum and the minima versus depth as Figure 7, but without removing surface magnetic regions. The result is shown in Figure 10. The $\delta\tau$ at the minima changes very little in comparison with that in Figure 7, as expected, while the $\delta\tau$ at the maximum changes significantly. The removal of the surface magnetic effect causes an increase in $\delta\tau$ at the maximum above the BCZ and a decrease around the BCZ. This change leads to that the $\delta\tau$ at the maximum is greater than that at the minima above the BCZ, while it is smaller around the BCZ, as shown in Figure 7. If the surface magnetic regions below 50G are also removed, it is expected that the $\delta\tau$ at the maximum would further increase above the BCZ and decrease around the BCZ. This would result in a greater change in the difference between the maximum and the minima from the region above the BCZ to the region around the BCZ. Therefore, the change in $\delta\tau$ at the maximum relative to the minima around the BCZ in Figure 7 cannot be caused by the residual of the surface magnetic effect.

To obtain the change in meridional flow velocity distribution from the minimum and the maximum, one needs to carry out inversion, which is nontrivial (Svanda et al. 2011; Svanda 2015). Here we give only an order-of-magnitude estimate for the depth dependence of meridional flow velocity based on the $\delta\tau$ in Figure 7, which is the average over 5°–20°. We assume the ray approximation and that the contribution of flow velocity to $\delta\tau$ is solely from the region around the lower-turning point. Thus, $\delta\tau$ is approximately related to the horizontal meridional flow velocity at the lower-turning point $\boldsymbol{v}_t$ as (Kosovichev 1996)

$$\delta\tau = 2\int \frac{\boldsymbol{v}\cdot d\boldsymbol{s}}{c^2} \approx 2\boldsymbol{v}_t \int \frac{1}{c^2}\, ds\ , \qquad (1)$$

where the second integral along the ray path is only over a range around the lower-turning point where the kernel is significant. The kernel is computed with the ray approximation and a standard solar model (Christensen-Dalsgaard et al. 1996). The estimate of $\boldsymbol{v}_t$ as a function of travel distance (depth), based on Equation (1) and the $\delta\tau$ at the maximum and the minima in Figure 7, is shown in Figure 11. It should be warned that this order-of-magnitude estimate could be rather different from correct inversion results. (For comparison, Giles 1999 obtained a flow velocity of about 5 m s^{-1} near the BCZ from inverting $\delta\tau$ averaged over 1996–1998, and Zhao et al. 2013 obtained about 10–15 m s^{-1} at 0.76 $R_\odot$ for a low-activity period.)

Like the time difference in Figure 7, the flow velocity in Figure 11 behaves differently at the maximum and the minima. The difference in the flow velocity between the maximum and the minima changes from the positive value above the BCZ to the negative value around the BCZ, and becomes about zero below the BCZ. The difference between the maximum and the minima changes about 10 m s^{-1} from the region above the BCZ to the region around the BCZ. This change in flow velocity is caused by the change in the physical conditions near the BCZ. We tend to attribute this change in physical conditions to the variation in magnetic field from the minimum to the maximum near the BCZ, because we cannot find other explanations for this change. However, it is a nontrivial task to infer the change in the magnetic field from the change in flow velocity because of the complicated relation between the flow velocity distribution and the magnetic field distribution. To obtain the change in the distribution of the magnetic field near the BCZ, in addition to the flow velocity distribution in the absence of magnetic field (at the minimum) and that in the presence of magnetic field(at the maximum), one needs a theory of interaction between the flow and the magnetic field to relate the change in flow velocity distribution to the change in magnetic field distribution for the whole convection zone. Their interaction with the differential rotation also needs to be included in the theory. The flow velocity distributions at the maximum and the minimum can be obtained by an inversion of the measured $\delta\tau$.

SOHO is a project of international cooperation between ESA and NASA. The sunspot data in Figures 1, 2, and 5 are from SIDC, Royal Observatory of Belgium. The authors are supported by the NSC of ROC under grant NSC-102-2112-M-007-022-MY3.

REFERENCES

Antia, H. M., Chitre, S. M., & Thompson, M. J. 2000, A&A, 360, 335
Baldner, C. S., & Basu, S. 2008, ApJ, 686, 1349
Baldner, C. S., & Schou, J. 2012, ApJL, 760, L1
Basu, S., & Antia, H. M. 2003, ApJ, 585, 553
Beck, J. G., Gizon, L., & Duvall, T. L., Jr. 2002, ApJL, 575, L47
Charbonneau, P. 2010, LRSP, 7 (http://www.livingreviews.org/lrsp-2010-3)
Chou, D.-Y., & Dai, D.-C. 2001, ApJL, 559, L175
Chou, D.-Y., & Ladenkov, O. 2005, ApJ, 630, 1206
Chou, D.-Y., Liang, Z.-C., Yang, M.-H., Zhao, H., & Sun, M.-T. 2009, ApJL, 696, L106
Chou, D.-Y., & Serebryanskiy, A. 2002, ApJL, 578, L157
Chou, D.-Y., & Serebryanskiy, A. 2005, ApJ, 624, 420
Choudhuri, A. R. 2011, Prama, 77, 77
Christensen-Dalsgaard, J., Dappen, W., Ajukov, S. V., et al. 1996, Sci, 272, 1286
Eff-Darwich, A., Korzennik, S. G., Jimenez-Reyes, S. J., & Perez Hernzndez, F. 2002, ApJ, 580, 574
Durney, B. R., & Roxburgh, I. W. 1971, SoPh, 16, 3
Duvall, T. L., Jr. 1979, SoPh, 63, 3
Duvall, T. L., Jr., D'Silva, S., Jefferies, S. M., Harvey, J. W., & Schou, J. 1996, Natur, 379, 235
Duvall, T. L., Jr., & Hanasoge, S. M. 2009, in ASP Conf. Ser. 416, Solar-Stellar Dynamos as Revealed by Helio- and Asteroseismology, (San Francisco, CA: ASP), 103
Duvall, T. L., Jr., Jefferies, S. M., Harvey, J. W., & Pomerantz, M. A. 1993, Natur, 362, 430
Dziembowski, W. A., & Goode, P. R. 1989, ApJ, 347, 540

Fan, Y. 2009, LRSP, 6 (http://www.livingreviews.org/lrsp-2009-4)
Giles, P. M. 1999, PhD thesis, Stanford Univ.
Giles, P. M., Duvall, T. L., Jr., Scherrer, P. H., & Bogart, R. S. 1997, Natur, 390, 52
Gizon, L., & Birch, A. C. 2002, ApJ, 571, 966
Haber, D. A., Hindman, B. W., Toomre, J., Bogard, R., & Larsen, R. 2002, ApJ, 570, 855
Hathaway, D. H., & Rightmire, L. 2010, Sci, 327, 1350
Hathaway, D. H., & Rightmire, L. 2011, ApJ, 729, 80
Howard, R., & Gilman, P. A. 1986, ApJ, 307, 389
Kholikov, S., & Hill, F. 2014, SoPh, 289, 1077
Komm, R. W., Howard, R. F., & Harvey, J. W. 1993, SoPh, 147, 207
Kosovichev, A. G. 1996, ApJL, 461, L55
Liang, Z.-C., & Chou, D.-Y. 2015, ApJ, 805, 165
Meunier, N. 1999, ApJ, 527, 967
Miesch, M. S. 2005, LRSP, 7 (http://www.livingreviews.org/lrsp-2005-1)
Ossendrijver, M. 2003, ARA&A, 11, 287
Scherrer, P. H., Bogart, R. S., Bush, R. I., et al. 1995, SoPh, 162, 129
Serebryanskiy, A., & Chou, D.-Y. 2005, ApJ, 633, 1187
Svanda, M. 2015, A&A, 575, A122
Svanda, M., Gizon, L., Hanasoge, S. M., & Ustyugov, S. D. 2011, A&A, 530, A148
Ulrich, R. K. 2010, ApJ, 725, 658
Usoskin, I. G., & Mursula, K. 2003, SoPh, 218, 319
Wang, Y.-M., Nash, A. G., & Sheeley, N. R., Jr. 1989, Sci, 245, 712
Zhao, J., Bogart, R. S., Kosvichev, A. G., Duvall, T. L., Jr., & Hartlep, T. 2013, ApJL, 774, L29
Zhao, J., & Kosvichev, A. G. 2004, ApJ, 603, 776
Zhao, J., Nagashima, K., Kosvichev, A. G., & Duvall, T. L., Jr. 2012, ApJL, 749, L5